Model-based concept to extract heart beat-to-beat variations beyond respiratory arrhythmia and baroreflex

Mindaugas Baranauskas[1*], Rytis Stanikūnas[2], Eugenijus Kaniušas[3], Arūnas Lukoševičius[1]

[1]Biomedical Engineering Institute, Kaunas University of Technology, Kaunas, Lithuania

[2]Institute of Psychology, Faculty of Philosophy, Vilnius University, Vilnius, Lithuania

[3]Institute of Biomedical Electronics, Vienna University of Technology, Vienna, Austria

*** Correspondence:**
Mindaugas Baranauskas
m.baranauskas@ktu.lt

Keywords: heart rate, beat-to-beat variations, neural regulation, modeling, personalization, respiratory arrhythmia, baroreflex, autonomic function

Abstract

Heart rate (HR) and its variability (HRV) reflect modulation of the autonomous nervous system, especially sympathovagal balance. The aim of this research was to develop a personalizable HR model and an in silico system that could identify HR regulation parameters associated with respiratory arrhythmia (RSA) and baroreflex, and subsequently capture residual heart beat-to-beat variations from individual psychophysiological recordings in humans. Here the respiration signal, blood pressure signal and time instances of R peaks of EKG are used as input for the model. The system extracts the residual displacements of the modeled R peaks relative to the real R peaks, considering the known lower-order mechanisms of the HR dynamics. Three components – tonic, spontaneous and 0.1 Hz changes – can be seen in these R peak displacements. These dynamic residuals can help analyze HRV beyond RSA and baroreflex, and our model-based concept suggests that the residuals are not merely modeling errors. The proposed method could help to investigate additional neural regulation impulses from the higher-order brain and other influences.

1 Introduction

The regulation of heart rate (HR) involves a number of hierarchical levels from the inner nervous system of the heart to the cerebral cortex (Palma and Benarroch, 2014; Schmaußer et al., 2022). Respiratory sinus arrhythmia (RSA) and cardiac baroreflex – two main lower-order HR regulation mechanisms – can explain the majority of *HR variability (HRV)* (Draghici and Taylor, 2016), however they overshadow other interesting time-varying influences as HRV components. Additionally, the respiration rate, age, sex and other factors must be considered (or be controlled) for a proper interpretation of HRV and for a comparison of HRV between individuals (Laborde et al., 2017; Shaffer and Ginsberg, 2017; Koenig et al., 2021).

The complex underlying regulation mechanisms and personal peculiarities are still not fully disclosed by traditional HRV measures, and other than traditional HRV measures are not always more helpful in the clinical context, although research on new ways to evaluate HR dynamics is still encouraged (Sassi et al., 2015)). *An alternative approach* would be to use statistical techniques to invert mathematically formulated forward models (Bach et al., 2018), or fitting HR dynamics to a

comprehensive personalizable HR regulation model to find weights of regulation mechanisms and analyze the residual HR dynamics unexplained by model.

Regulation at *lower levels* are more deterministic, more investigated and numerous models of heart regulation, tried to include this knowledge, for example, models of Ursino (1998) and its extensions (Ursino and Magosso, 2000; Hsing-Hua Fan and Khoo, 2002; Magosso et al., 2002; Cheng et al., 2010; Albanese et al., 2016; Park et al., 2020), Kotani et al (2005) and it's derivations (e.g., Ishbulatov et al., 2020), and other closed-loop models (Van Roon et al., 2004; Ortiz-León et al., 2014) and specific purpose open loop models (Randall et al., 2019) for humans. Additional linkage of the model with registered biosignals would make the model adaptive and *personalizable*.

We also propose that HR variations unexplained by lower-order mechanisms (at least RSA and cardiac baroreflex) could be interpreted/used as an enhanced 'signal / noise' ratio while trying to capture other influences, for example, associated with higher-order brain regulation mechanisms versus other influences. Activity in the higher brain areas has complex interactions, outcomes of activity in some higher-order brain structures have associations with specific autonomous nervous system (ANS) branches, for example, parasympathetic influence could come from ventromedial prefrontal cortex (Wong et al., 2007; Ziegler et al., 2009; Schmaußer et al., 2022), right (Coote, 2013) or/and anterior (Chouchou et al., 2019) insular cortex, and sympathetic influence could come from left (Oppenheimer et al., 1992; Coote, 2013) or/and posterior (Chouchou et al., 2019) insular cortex, locus coeruleus (Mather et al., 2017). The effect of a single parasympathetic impulse on HR is very fast and could vanish within one second (Spear et al., 1979; Berger et al., 1989), thus HR modeling preferably should be done with cardiac cycle to align parasympathetic bursts. However, known personalization solutions (Olufsen and Ottesen, 2013; Randall et al., 2019) use mean arterial blood pressure (ABP) – not a continuous ABP signal with changes within the interbeat period. More granular timing could also help extract higher-order HR regulation since brain stimulation correlates with HRV measures sensitive to fast changes in HR, e.g., high-frequency power (Schmaußer et al., 2022), however standard HRV measures usually generalize several minutes of psychophysiological data (Shaffer and Ginsberg, 2017). To our knowledge, there is still no computational psychophysiologically based personalizable model of HR regulation that considers ANS activity fluctuations within the cardiac cycle.

The *aim* of our article was to develop a computational model-based method that could identify heart rate regulation parameters associated with respiratory arrhythmia and baroreflex, and subsequently capture the remaining heart beat-to-beat variations from individual empirical human psychophysiological recordings.

First, a comprehensive computational HR lower order neural control model for RSA and baroreflex is constructed. Subsequently, a system for personalization of the model parameters is presented through the use of experimental signals. Results showing residual HR variations beyond RSA and baroreflex possibly attributable to higher-order brain control are shown and discussed.

2 Methods

The HR regulation model encompasses three main domains: 1) heart, 2) brain lower and higher order neural control, and 3) vasculature (see **Figure 1**). The respiratory system could be interpreted as a lower-order neural control subdomain if considered as a neural respiration center (due to link to NAmb). The general scheme of the main HRV mechanisms – RSA (respiration center, *nucleus ambiguus* (NAmb), X cranial nervus vagus, sinoatrial node (SAN)) and baroreflexes (baroreceptors, *nucleus tractus solitarius* (NTS), NAmb for vagal effects; baroreceptors, NTS, rostral ventrolateral medulla (RVLM), intermediolateral column (IML) for sympathetic effects) – are inspired by Feher

This is a provisional file, not the final typeset article

(2017, 613, his Figure 5.13.6) and Jänig (2006, 401). Most modules of this general scheme have a more detailed internal algorithmic structure described in dedicated parts of Chapter 2.1. The respiration signal, ABP signal and time instances of the real R peaks of EKG are used as input for the model. The HR model outputs the modeled R peaks and sympathetic nerve activity (SNA). The HR model itself implements the alignment of the real and modeled R peaks needed for the later extraction of the residual HR variations – that is, the displacements of the modeled R peaks relative to real R peaks – outside the model.

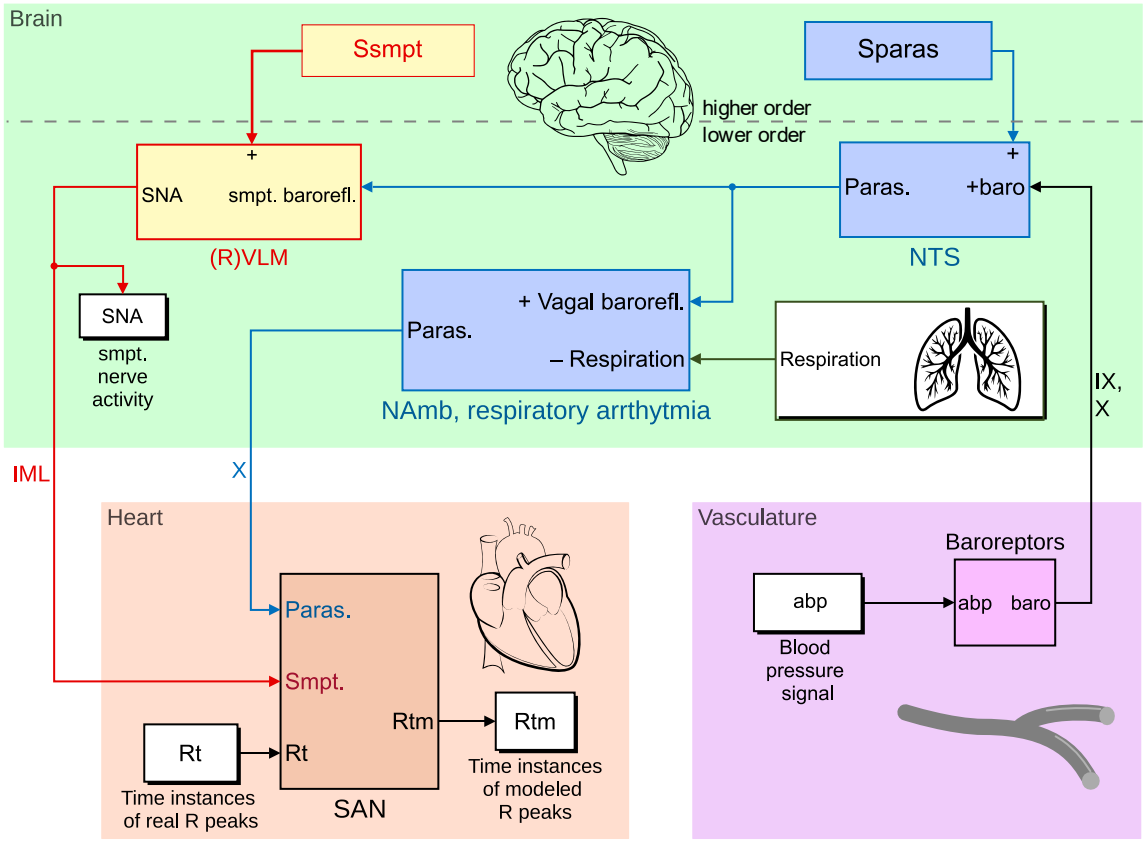

Figure 1. Heart rate regulation model overview scheme in Simulink. It encompasses three main domains: 1) heart (orange), 2) brain (green) – higher-order neural control, also lower-order neural control through respiratory sinus arrhythmia and baroreflex, and 3) vasculature (pink). Abbreviations of structures: IML, intermediolateral column; IX, nervus glossopharyngeus; NAmb, nucleus ambiguus; NTS, nucleus tractus solitarius; (R)VLM, (rostral) ventrolateral medulla; SAN, sinoatrial node; X, nervus vagus. Other abbreviations: baro, activity of baroafferents; paras, parasympathetic activity; smpt, sympathetic activity; Sparas, higher-order parasympathetic activity; Ssmpt, higher-order sympathetic activity. Most modules of this general scheme have more detailed internal algorithmic structure described in a dedicated sub-chapter.

For empirical psychophysiological data fitting to the HR regulation model, the processed psychophysiological signals (procedure described in Chapter 2.3.2) and manually configured set of various parameters (e.g., lower and upper boundaries of the parameters of the HR regulation model) are passed to optimization algorithms (see left side of **Figure 2**) to find the set of model parameters with minimal error score. The calculation of the error score is based on the R peak displacements in time and SNA. The system for personalization of the model parameters is described in Chapter 2.2.

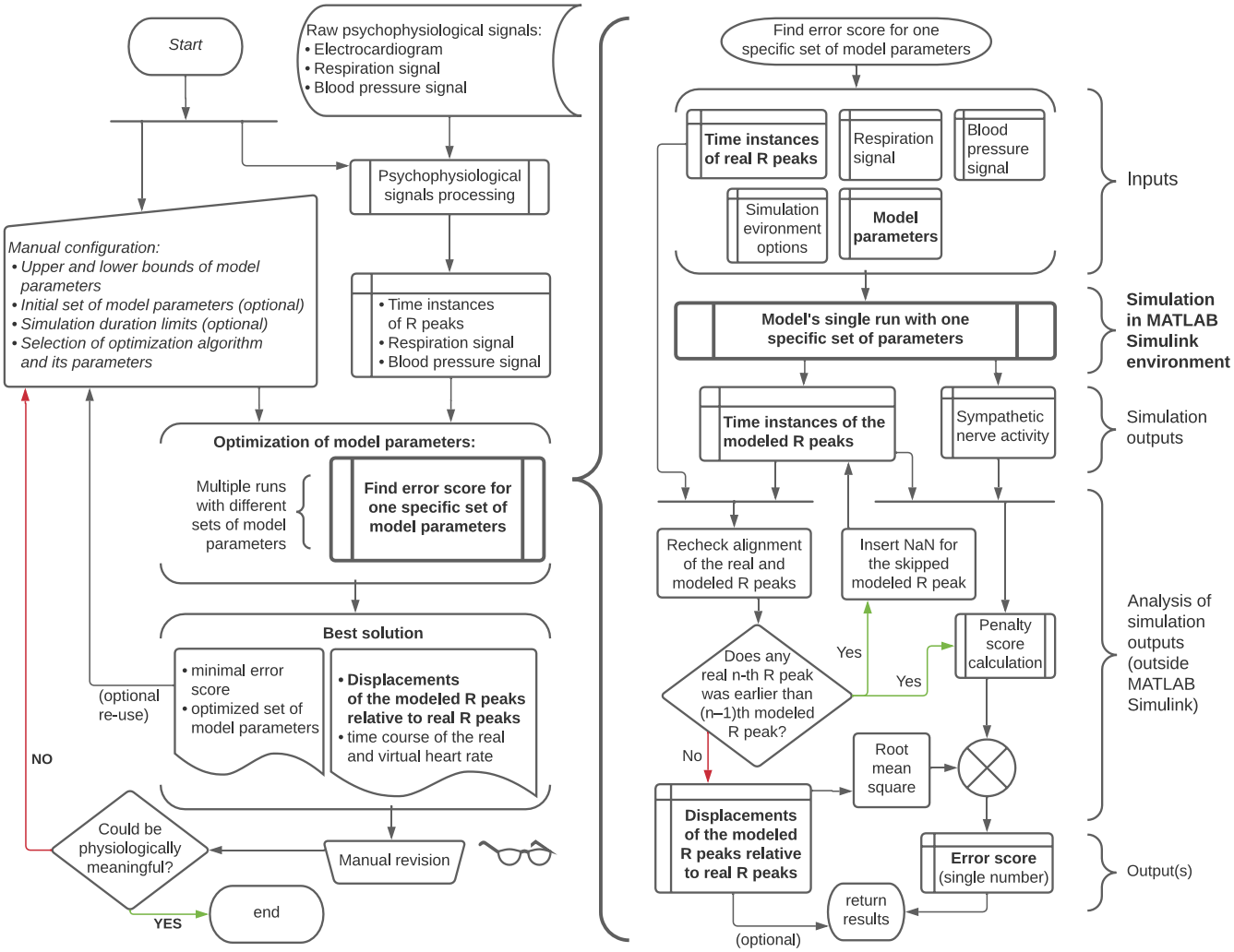

Figure 2. Algorithmic scheme of concept. Here 'model' (and "Model's single run with a specific set of parameters") refers to the heart rate regulation model realized in MATLAB Simulink environment. Although this model usually returns the modeled R peaks aligned to the real ones, re-check and correction is needed for rare cases of the skipped modeled R peak(s). NaN, not a number.

The model is implemented in MATLAB Simulink environment and runs with ODE3 (Bogacki-Shampine) solver and fixed step of 1 milisecond. The computational system "Ritminukas" implementing this model-based concept can be downloaded from the open source Zenodo repository: <https://doi.org/10.5281/zenodo.7765459>.

2.1 Heart rate (HR) regulation model

2.1.1 Heart: Sinoatrial node – Integration of parasympathetic and sympathetic activity

The pharmacologically blocked or denervated during transplantation HR generated at SAN is practically constant for person (Jose and Collison, 1970; Zeuzem et al., 1991), however, it slowly decreases with age (Jose and Collison, 1970). In our HR regulation model, this *pacemaker* frequency is included as *HRbasal* variable (see **Figure 3**). If age is known, *HRbasal* can be defined by the Jose and Collison (1970) formula:

$$\boldsymbol{HRbasal} = (\mathbf{118.1} - \mathbf{0.57} \times \boldsymbol{age}) \pm \mathbf{8}$$

This is a provisional file, not the final typeset article

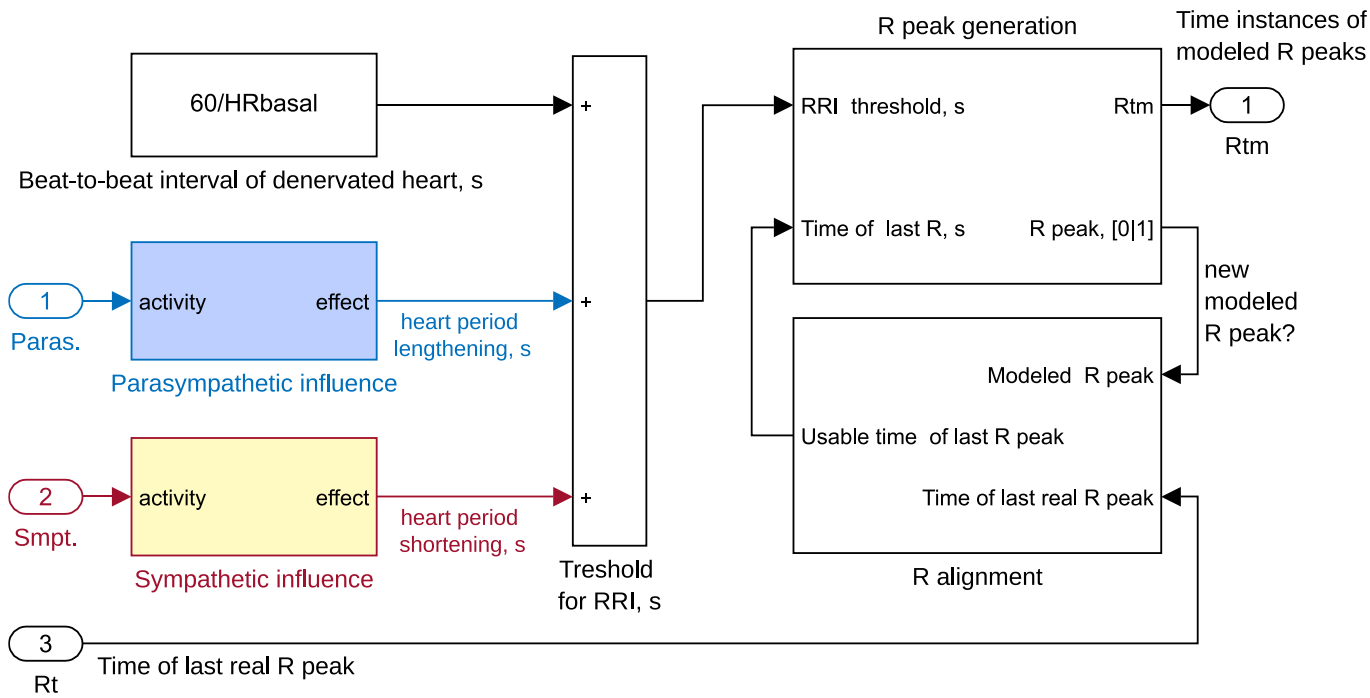

Figure 3. Sinoatrial node block scheme in Simulink. New R peaks are modeled when a time threshold for R-R intervals (RRI) is reached, which is calculated with respect to the real R peak time instances; that is time instances of last real R peak are used to align real and modeled R peaks and find the lack or surplus of threshold for each R peak time during analysis outside the model;. *HRbasal* – pacemaker's internal frequency; Paras, parasympathetic activity; Rtm, time instances of modeled R peaks; Smpt, sympathetic activity.

Thus, for model parameter optimization we allow deviation up to 8 bmp from this computed value.

The SAN is innervated by the X cranial nerve (vagus) providing *parasympathetic input* and IML of the spinal cord providing *sympathetic input* (Palma and Benarroch, 2014) (see **Figure 1**, **Figure 3** to see its place in our model). Parasympathetic burst decelerates HR with delay of about 0.2 s, the strongest effect is at approximately 0.5 s after the stimulation and vanishes after 1 s; meanwhile, sympathetic burst accelerates the HR with delay of about 1-2 s (we set 1.5 s), the strongest effect is at approximately 4 s and vanishes at 20 s after the stimulation. We use custom made transfer function based on Spear (1979, their Figure 2) and Berger et al (1989, their Fig 4) empirical data for parasympathetic (see **Figure 4**) and sympathetic (see **Figure 5**) neural burst effect on heart period. Unlike Ursino (1998) and similar models where single first-order transfer function suggests exponential-like autonomic nervous system effect on heart period, here we use difference of two transfer functions to achieve gradual effect before its peak. In our SAN block, we use R-R intervals (RRI) instead of HR, because parasympathetic and sympathetic activity (burst frequency) influence on RRI is almost linear (Draghici and Taylor, 2016; Geus et al., 2019).

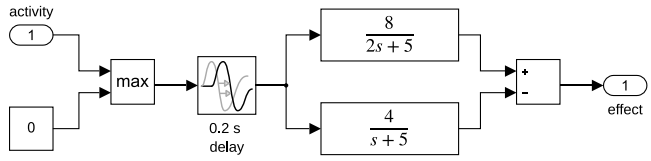

Figure 4. Parasympathetic influence sub-block of sinoatrial node block in Simulink.

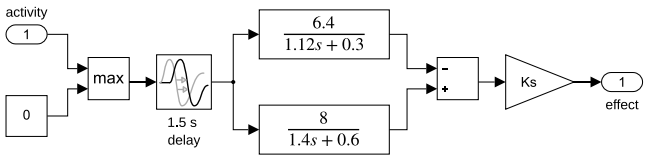

Figure 5. Sympathetic influence sub-block of sinoatrial node block in Simulink. Ks, sympathetic activity coefficient.

The time-varying threshold for RRI is obtained by summing the heart period of the denervated heart (60/*HRbasal*) and the parasympathetic and sympathetic effects mentioned above (see **Figure 3**). When the accumulated time after the last R peak is more than 300 ms and hits the dynamically changing RRI threshold, the pacemaker fires (a new R peak is generated) and is immediately reset to zero in the "EKG R peak generation" sub-block (see **Figure 3** and **Figure 6**). Here, time instances of modeled R peaks are stored in memory for analysis outside the model.

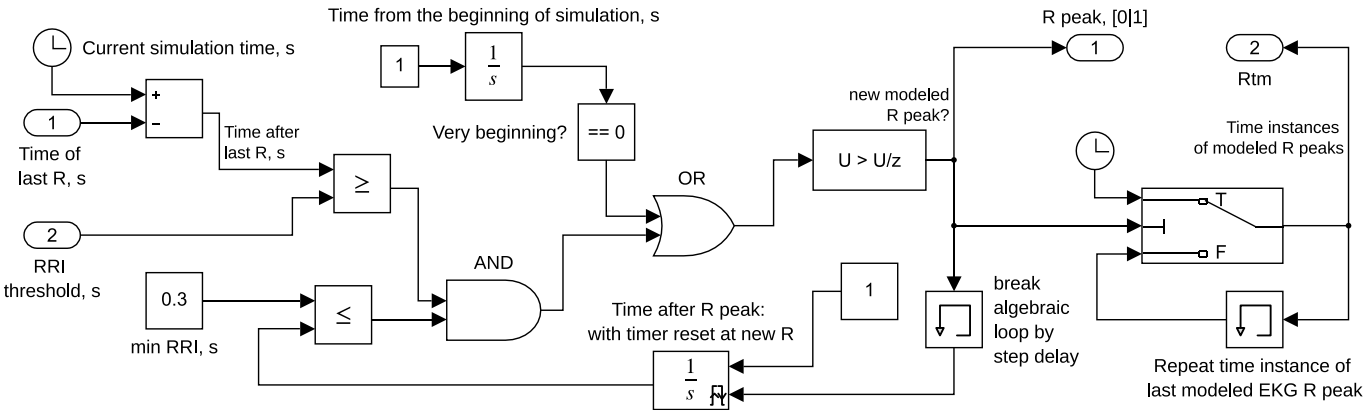

Figure 6. EKG R peak generation sub-block in Simulink. When the accumulated time after the last R peak is more than 300 ms and hits the dynamically changing R-R interval (RRI) threshold, the pacemaker fires (a new R peak is generated) and is immediately reset to zero. Note 1: 'current simulation time' and 'time from the beginning of simulation' will not be the same if simulation starts not at zero second of psychophysiological recording. Note 2: 'time instances of modeled R peaks' are not be the same as 'time of last R' because R alignment is enabled outside this sub-block. Time instances of modeled R peaks are passed to be stored in memory (here 'Rtm') for analysis outside model.

The key part in this HR model is the sub-block for the alignment of the real and modeled R peaks (see **Figure 6** for its context within the SAN sub-block, and **Figure 7** for its detailed implementation in Simulink). Usually, this block returns the time instance of the previous real R peak as output for the corresponding modeled R peak; however, if the modeled R peak, precedes the real R peak then infinity will be temporarily returned as the 'usable time of the last R peak' - new modeled R peaks will be blocked - until reset by the next real R peak; if the real R peak preceded the modeled R peak, then the update of the output value will be blocked until the new modeled R peak. This allows one to model R peaks relative to time instances of the real R peaks. Besides, this approach enables to extract the R displacements by comparing real and the modeled EKG R peaks outside the model. However, this sub-block cannot deal with cases when the modeled R peak happens later than one real R peak; the additional re-check and correction of these cases outside the model is described in Chapter 2.2.

This is a provisional file, not the final typeset article

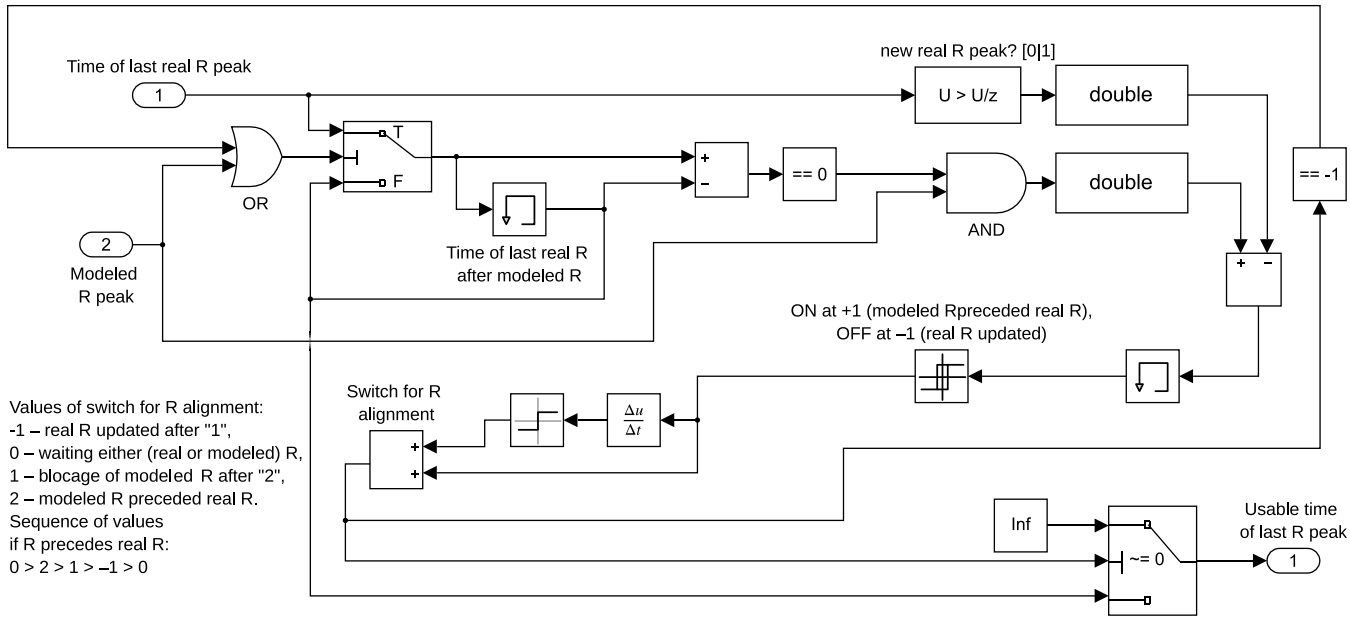

Figure 7. Simulink sub-block for alignment of the real and modeled R peaks.

2.1.2 Vasculature: Baroreception

The blood pulse wave stretches the vessel walls and reaches the arterial baroreceptors in the aortic arch and carotid sinus after 10-15 ms and 40-65 ms respectively, that is, about 90 ms and 140 ms after the R peak in the EKG respectively (Edwards et al., 2009; Wehrwein and Joyner, 2013; Martins et al., 2014). Stimulation of aortic and carotid baroreceptors can have different impacts on HR control (Ishii et al., 2015), however, we don't differentiate between them. We modeled the integrated baroreceptor activity and set an average delay of 30 ms (see **Figure 8**). Some baroreceptors react more to phasic changes of ABP, while some others more react to absolute level of ABP. Thus, for integration, we add the derivative of ABP by the coefficient *Pk* and scale the resulting sum by *Kb*. Baroreceptors may take about 20 ms to react to ABP (Borst and Karemaker, 1983) and the integrated baroreceptor activity peak is estimated at about 250 ms and extinguish until 390 ms after the EKG R (Edwards et al., 2009), thus, to match this with experimental or simulated data, we add 50 ms time lag for modified ABP signal *P* in our model. Baroreceptors (regardless of their place) have different activation thresholds, response functions, and saturation levels (Wehrwein and Joyner, 2013; Feher, 2017, 610), thus, to generate within cardiac cycle varying baroafferent activity (*baro*), we use sigmoidal function which is similar to the used in Ursino (1998) model:

$$\boldsymbol{baro} = \frac{\boldsymbol{Bmax} \cdot \boldsymbol{e}^{\frac{\boldsymbol{P-Peq}}{\boldsymbol{Kab}}}}{\boldsymbol{1} + \boldsymbol{e}^{\frac{\boldsymbol{P-Peq}}{\boldsymbol{Kab}}}}$$

where *Peq* is the central point of the sigmoidal functional, *Kab* – slope-related coefficient, *Bmax* – saturation level (could be sensitive to postural position). Unlike Ursino (1998), we did not set a minimal activation level since most baroreceptors do not show spontaneous activity, and instead we set tonic parasympathetic activity coming from the higher order brain areas to NTS (see **Figure 1**). The values of baroreception parameters are suggested to be selected so that the baroreceptors would be more sensitive to the main pulse front and less sensitive to the dicrotic notch.

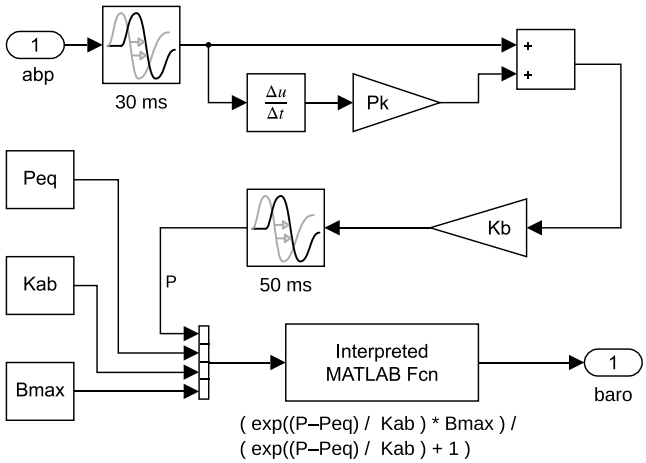

Figure 8. Simulation of the integrated baroreceptor responses (baro) from arterial blood pressure (abp) signal in Simulink. Bmax, saturation level of baroafferent activity; Kab, slope-related coefficient for baroreception; Kb, scaling factor of *abp* and its derivative sum for baroreception; Peq, central point of the sigmoidal functional for baroreception; Pk, *abp* derivative coefficient for baroreception.

2.1.3 Brain

2.1.3.1 Path through NTS for cardiac vagal and sympathetic baroreflexes

Baroreceptive information from the carotid and aortic baroreceptors travels via cranial nerves – glossopharyngeal and vagus, respectively – and reaches the NTS in 10-15 ms (Wehrwein and Joyner, 2013; Martins et al., 2014). NTS is the first central relay station of visceral afferent information and is part of the circuit for all medullary reflexes, including the baroreflex (Palma and Benarroch, 2014). NTS projects within 100 to 150 ms to areas responsible for baroreflex effects, including NAmb and RVLM, that is, about 200 to 300 ms after the R peak in EKG (Edwards et al., 2001). Thus, we add 15 and 125 ms time delays, respectively, as the fixed values in the NTS scheme (see **Figure 9**).

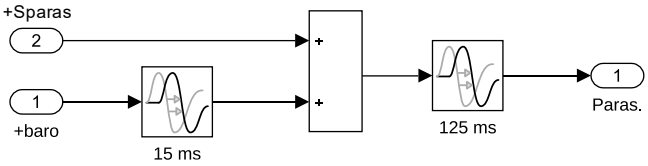

Figure 9. Nucleus tractus solitarius scheme in Simulink. Abbreviations: baro, activity of baroafferents; Paras, parasympathetic activity for output; Sparas, higher-order parasympathetic activity for input.

NTS is under powerful control of the brain, integrates afferent information, and sends projections back almost to same great variety of neural structures, including the brainstem, amygdala, and (via thalamus) insular and prefrontal cortices (Jänig, 2006, 311–317). In this HR model, the NTS is set not to have spontaneous activity and to receive the integrated parasympathetic excitatory input *Sparas* from the 'brain' (see **Figure 1** and **Figure 9**), and NTS is also the only structure to receive this input.

Baroreflex acts via NTS in three ways: as cardiac vagal (parasympathetic) baroreflex (via NAmb, see 2.1.3.2 subchapter), cardiac sympathetic baroreflex (via RVLM, see 2.1.3.3 subchapter), and noncardiac sympathetic baroreflex (not relevant to our HR model). In the cardiac vagal baroreflex circuit, NTS directly excites preganglionic cardiac vagal neurons in NAmb, resulting in HR deceleration (Wehrwein and Joyner, 2013; Palma and Benarroch, 2014).

This is a provisional file, not the final typeset article

2.1.3.2 Preganglionic cardiac vagal neurons in the nucleus ambiguus (NAmb) and respiratory sinus arrhythmia (RSA)

The majority (about 80%) of preganglionic cardiac neurons originate from NAmb, effectively decelerate HR via myelinated fibers, and their activity usually is mostly similar to the respiration pattern (Coote, 2013); effect of other cardiac vagal neurons is relatively small, more delayed, and slower than those of NAmb (Coote, 2013). NAmb neurons are not spontaneously active themselves – they are excited by other areas of brainstem, predominantly by the NTS, and are inhibited by neurons of the medullary ventral respiratory group ('respiration center') only during inspiration, that is, they are not blocked during expiration or holding of breath, apnea (Dergacheva et al., 2010; Palma and Benarroch, 2014; Feher, 2017, 612–613), though this inhibition is not complete and does not imply absence of inhibition later (Geus et al., 2019). The aggregated effect causes RSA – a temporal withdrawal of the predominant parasympathetic activity that causes the acceleration of HR during inspiration. Therefore, we include only preganglionic cardiac neurons of NAmb with excitatory input from NTS (incorporating baroreceptive information) and inhibition by multiplication of the square root of the derivative of the respiration signal and transfer function with *Krsa* and *Drsa* parameters only at inspiration (see **Figure 10**). The NAmb output activity is set to be always non-negative.

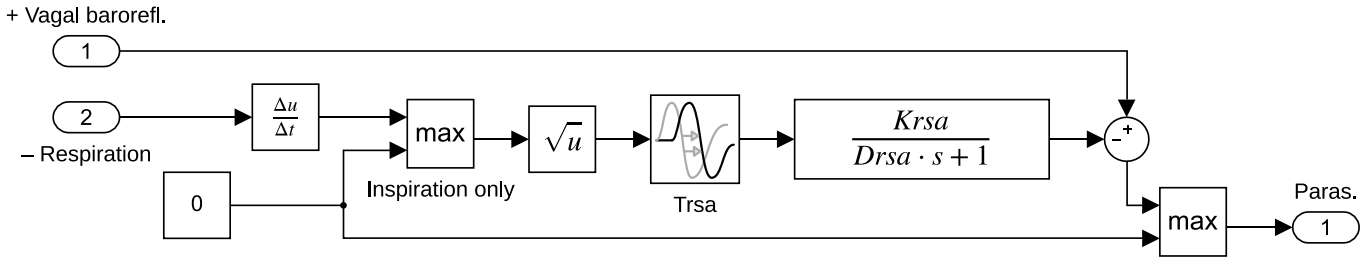

Figure 10. Nucleus ambiguus scheme for *respiratory arrhythmia* in Simulink. Parasympathetic activity ('Vagal baroreflex' input #1) is inhibited during inspiration with little time delay *Trsa*. Inhibition strength depends on respiration (input #2) signal derivative (its square root), transfer function (where *Drsa* is in denominator), and custom *Krsa* coefficient. Block outputs parasympathetic activity (Paras.).

2.1.3.3 Rostral ventrolateral medulla (RVLM) for sympathetic baroreflex

The aggregated effect of baroreceptor stimulation inhibits sympathetic activity. In sympathetic baroreflex circuit, NTS through the caudal ventrolateral medulla (CVLM) or directly inhibits RVLM (Wehrwein and Joyner, 2013; Palma and Benarroch, 2014). Thus, in our model overview scheme NTS is shown to act on '(R)VLM' (see **Figure 1**).

Sympathetic baroreflex does not produce sympathetic outflow by itself: if central sympathetic activity would be low or insufficient (e.g., during anesthesia), sympathetic baroreflex will not be noticeable (Karemaker, 2022). RVLM has spontaneous activity itself and receives various excitatory inputs (Jänig, 2006, 393–396). Sympathoexcitatory RVLM neurons are activated by psychological stress, pain, hypoxia, hypovolemia, and hypoglycemia both directly and via descending inputs from higher-order structures (e.g., insula, prefrontal cortex, amygdala, and hypothalamic subnuclei) (Palma and Benarroch, 2014; Barman and Yates, 2017). In this HR model, the RVLM theoretically has constant spontaneous activity *Arvlm_sp* and receives the integrated sympathetic excitatory input from 'brain' *Ssmpt* (see left side of **Figure 11** and sub-chapter 2.1.3.4 below) – RVLM is also the only structure receiving such input.

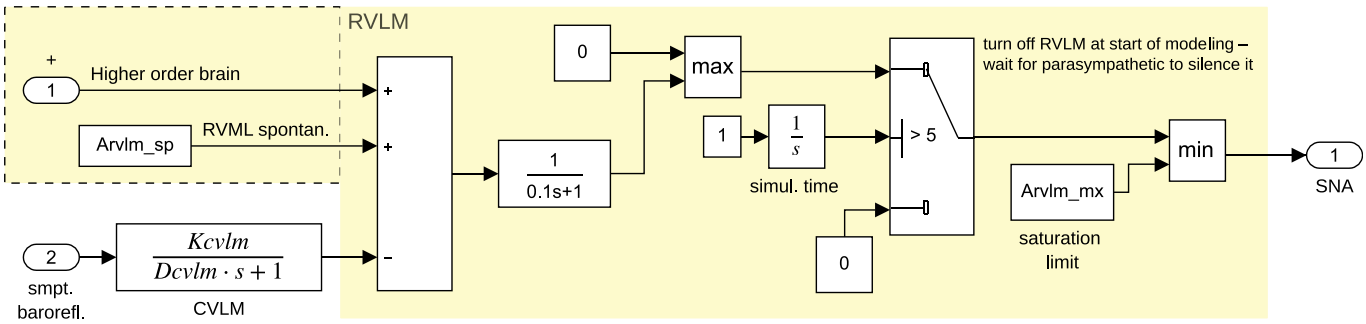

Figure 11. Rostral ventrolateral medulla (RVLM) algorithmic structure in Simulink to generate pulsatile sympathetic nerve activity (SNA) when it is not fully blocked by the caudal ventrolateral medulla (CVLM). Variables: *Arvlm_sp* – constant spontaneous RVLM internal activity, *Arvlm_mx* – saturation limit of RVML output; *Dcvml* and *Kcvml* – NTS parasympathetic effect on sympathetic activity coefficient.

The RVLM output has a pulsatile pattern and it is seen when it is not blocked by NTS/CVLM. Inhibition of NTS/CVLM activity itself seems to be too short to achieve only short RVLM impulses when the tonic NTS/CVLM level drops. How exactly this happens in the ventrolateral medulla is not known; thus we implement two first-order transfer functions to obtain a closer to desired effect; only one of these transfer functions has variable parameters (*Kcvlm* and *Dcvlm*) and is simply conventionally named as CVLM (see **Figure 11**).

The just started model would produce long-term lasting strong sympathetic effects on heart rate and vasculature, therefore, we temporarily turn off RVLM for 5 seconds until parasympathetic activity through NTS/CVLM would regularly inhibit RVLM and limit RVLM output to saturation value *Arvlm_mx* (see right side of **Figure 11**).

The SNA generated by RVLM travels through sympathetic IML of the spinal cord; IML neurons serve as a common sympathetic effector and through sympathetic ganglia innervate blood vessels (non-cardiac (arterial) sympathetic baroreflex, which is not relevant to our HR model) and the heart (cardiac sympathetic baroreflex) (Wehrwein and Joyner, 2013; Palma and Benarroch, 2014). Cardiac sympathetic baroreflex effect on withdrawal of sympathetic HR acceleration described in Chapter 2.1.1).

2.1.3.4 Higher-order regulation

The intrinsic HR is about 40 bmp faster than the mean HR in the resting state due to dominance of parasympathetic influence (Smetana and Malik, 2013) and higher-order brain regulation is critical to maintain it, e.g., by salience network (were anterior insular and anterior cingulate cortices the core of it) (Guo et al., 2016) and (pre-)frontal cortex (Wong et al., 2007; Thayer and Lane, 2009; Ziegler et al., 2009; Smith et al., 2017). The mere thickness of the prefrontal cortex and insula is positively correlated with the resting HRV (Koenig et al., 2021). In our model, this higher-order parasympathetic activity is included as the *Sparas* parameter (see **Figure 1**).

Theoretically, the tonic sympathetic activity could be set as the *Ssmpt* parameter (see **Figure 1**), however, during parameter optimization we cannot differentiate *Arvlm_sp* and *Ssmpt*, thus we practically set *Ssmpt* = 0 and *Arvlm_sp* means a constant sum of RVLM spontaneous activity and sympathetic excitatory input from the 'brain' (see **Figure 11** and sub-chapter 2.1.3.3 above).

2.2 System for model personalization

Although the HR regulation model usually returns the correctly aligned real and modeled R peaks, rechecking and correction is needed for rare cases of the skipped modeled R peak: if the real n^{th} R

This is a provisional file, not the final typeset article

peak was earlier than (n–1)th modeled R peak, then *NaN (not a number)* must be inserted for the skipped modeled R peak (see right side of **Figure 2**).

Based on the displacements of the modeled R peaks relative to the real R peaks and the SNA, the error score is calculated. The error score is used for its minimization during parameters optimization and is calculated only for a period starting 30 seconds after the beginning of the simulation. The error score is the sum of two components listed below (see also the right side of **Figure 2**):

1. *root mean square (RMS) of R peaks displacements* (i.e., RMS of time instance differences between the real R peaks and the corresponding aligned modeled R peaks) in milliseconds;
2. *penalty score* which consists of:
    - penalty of 200 × the ratio of the skipped modeled R peaks and all real R peaks within the analysis period; this penalty is added only if this ratio > 5%;
    - penalty due to the integrated SNA properties by summing (up to maximum sum of 250):
        - penalty of 50 – if any SNA lower peak is higher peak > 0;
        - penalty of 50 – if SNA saturates for longer than 0.3 s uninterruptedly;
        - penalty of 50 – if the ratio of unique SNA values and the number of all real R peaks within the analysis period < 10%;
        - penalty of 100 × (SNA peak relative to the R peak as found by cross-correlation – 0.8) – only if the SNA peaks are greater than 0.8 s after the R peaks;
        - penalty of 200 – if SNA is zero all the time.

Since optimization algorithms hardly can find the global minimum, and the lowest local minimum may not be psychophysiologically meaningful by the combination of parameters (as a whole, or due to stuck at floors or ceils of boundaries) or by the morphology of the modeled R peaks, several invocations of these optimization algorithms may be needed to find out the most acceptable local minimum (see left side of **Figure 2**). Therefore, the best optimized solutions must be manually reviewed.

For personalization of HR model parameters, the selected initial bounds of parameters are provided in **Table 1**. In total, 15(-16) model parameters could be personalized (16th *Ssmpt* is theoretical, practically not used). Lower and upper boundaries or initial values for several of them could be roughly estimated by physiological norms (e.g., *HRbasal* by knowing age) or from other models having similar components (e.g., *Peq* and *Kab* from Ursino (1998) model); boundaries for remaining parameters suggested by our internal manual research (see **Table 1** for summary) to avoid often stuck at boundaries during parameter optimization and to avoid too often search in too broad range leading to the wrong optimization result, e.g., to avoid the modeled HR being constant at mean of the real HR.

Optimization of HR regulation model parameters is done with MATLAB *particleswarm* and *patternsearch* algorithms from Global Optimization Toolbox: first, for initial random selection of model parameters, and later, to find more precise solution with minimal error score. Successful optimization required to change *the parameters of the* '*patternsearch*' optimization algorithm from the defaults: tolerance on the function ('FunctionTolerance') set to 0.001, i.e. to stop iterations if the change in function value is less than 0.001; tolerance on the variable ('StepTolerance') to stop iterations if both the change in position and the mesh size are less than 0.001; polling strategy used in the pattern search ('PollMethod') set to GSSPositiveBasis2N (which is similar to the default GPSPositiveBasis2N, but GSSPositiveBasis2N is more efficient than GPSPositiveBasis2N when the

current point is near a linear constraint boundary); order of poll directions in pattern search ('PollOrderAlgorithm' changed to "Random"; complete poll around the current point ('UseCompletePoll'). The parameter of the '*particleswarm*' optimization algorithm changed from the default: 'FunctionTolerance' set to 0.001, i.e. to end iterations when the relative change in the best objective function value over the last 20 iterations is less than 0.001. One invocation of the selected optimization algorithm runs the HR regulation model multiple times, each time with a different set of HR model parameters.

Table 1. Summary of the parameters of the personalizable heart rate regulation model. Abbreviations: ABP, arterial (blood) pressure; CVLM, caudal ventrolateral medulla; NAmb, nucleus ambiguus; NTS, nucleus tractus solitarius; RSA, respiratory sinus arrhythmia; (R)VLM, (rostral) ventrolateral medulla; SAN, sinoatrial node.

Mechanisms: Domain	**Parameter name**	**Range for optimization**	**Personalized value**		**Units**	**Description**
			33y subj.	**50y subj.**		
All: Brain	Sparas	[0 1]	0.014605	0.116169	–	Basal level of the parasympathetic activity from (higher-order) brain
All: Heart/SAN	HRbasal	[70 120]	107.6261	83.02557	beats/min	Rate of denervated heart at SAN.
RSA: Brain/NAmb	Drsa	[0.4 2.5]	0.767133	1.226438	–	Transfer function denominator at NAmb for RSA
	Krsa	[0 2]	0.250125	0.182839	–	RSA coefficient at NAmb
	Trsa	[0 1]	0.544354	0.540044	s	Time delay between the respiration signal and RSA effect
Sympathetic baroreflex: Brain	Ssmpt	0	0	0	–	Theoretically, the basal level of the sympathetic from (higher-order) brain, practically merged with *Arvlm_sp* and thus here set to 0
Sympathetic baroreflex: Brain/(R)VLM	Arvlm_sp	[0 5]	1.692973	4.651536	–	Theoretically, only constant spontaneous RVLM internal activity, practically brain sympathetic basal level is added
	Arvlm_mx	[0.001 0.5]	0.063362	0.456075	–	Saturation limit of RVML output
	Kcvlm	[0 30]	6.644312	27.55722	–	NTS parasympathetic effect on the sympathetic activity coefficient at CVLM
	Dcvlm	[0.1 1]	0.100638	0.10884	–	Transfer function denominator at CVLM
Sympathetic baroreflex: Heart/SAN	Ks	[0 10]	1.952591	0.272138	–	Sympathetic activity coefficient at SAN
Vagal and sympathetic baroreflexes: Vasculature/ Baroreceptors	Pk	[0 5]	0.30804	0.888058	–	ABP derivative coefficient for baroreception
	Kb	[0.01 10]	2.302123	2.749199	–	Scaling factor of ABP and its derivative sum for baroreception
	Peq	[80 100]	89.19561	82.82140	mmHg	Central point of the sigmoidal functional for baroreception
	Kab	[1 50]	17.72824	16.47293	–	Slope-related coefficient for baroreception
	Bmax	[0 5]	0.450024	0.107924	–	Saturation level of baroafferent activity

This is a provisional file, not the final typeset article

2.3 Testing of a model-based concept

2.3.1 Participants, equipment, and procedure

Two healthy male participants (aged 33 and 50, without any heart-related problems) volunteered in the pilot recordings to fit our HR model. These pilot recordings were conducted in accordance with the ethical principles of the Declaration of Helsinki, including written informed consent and voluntary participation.

Psychophysiological recordings were performed with BIOPAC MP150 (Biopac Systems Inc., 42 Aero Camino, Goleta, CA, United States) with ECG electrodes placed according to lead II and respiration belt on abdomen. ABP was registered with the Portapres device (Finapres Medical Systems BV, Palatijn 3, Enschede, Netherlands) using finger cuffs.

The participants were in the supine position for 10 min of rest, followed by slow breathing for 3 min and again 10 min rest.

2.3.2 Offline signal processing

The *EKG* signal was 0.4–35 Hz band-pass filtered offline using Butterworth filter. Time instances of EKG R peaks were identified from the EKG signal using a modified Pan-Tompkins (1985) algorithm and were additionally visually inspected together with the raw EKG signal. Wrongly detected R peaks were manually corrected by selecting the real EKG R time as signal peak or interpolated.

The respiratory signal was low-pass filtered with cut-off at 0.4 Hz and normalized between –0.5 and 0.5.

Since *ABP was* registered on the fingers of the hand, the ABP signal was shifted by –100 ms to compensate blood arrival time difference between baroreceptors and fingers. The ABP signal was low-pass filtered with cut-off at 10 Hz. The baseline was changed to 80 mmHg.

2.3.3 Derived psychophysiological data

Additional psychophysiological data were derived for a more comprehensive visualization of the results. To see the HR variations together with respiration signal, the real HR was directly derived from time instances of the R peaks. Meanwhile, virtual HR was derived from difference between the real RRI and the corresponding R peak displacements (not by using RRI from the modeled R peaks). To see the associations of ABP with baroreflex-mediated SNA and HR variations, systolic and diastolic blood pressures were derived as upper and lower envelopes of the processed ABP signal. The standard deviation of RRI (SDNN) for the entire 23 min record was computed to evaluate general HRV.

2.3.4 Additional details on the fit of psychophysiological data to model

For parameter personalization, the HR model has been run across the entire 23-minute length of empirical psychophysiological records on MATLAB R2022b parallel pool of 45 processes in a computer with AMD Ryzen Threadripper PRO 5995WX 64-Cores 2.70 GHz processor, 128 GB RAM.

3 Results

The processed experimental psychophysiological data was fitted to the HR regulation model by evaluating multiple sets of parameters to find a solution with minimal error score, i.e., the sum of minimal RMS of R peak displacements and the penalty score.

Optimization of HR model parameters was called twice with the *particleswarm* algorithm and once with the *patternsearch* algorithm – after each invocation passing the best solution for the next optimization as initial set. For the parameter personalization of a 33-year-old male, in total 11859 evaluations of the sets of model parameters in Simulink took about 3 hours and 11 minutes to obtain the most optimal solution with RMS of R peak displacements 49.051 ms for a time period from 30 s to 23 minutes (SDNN of real RRI was 88.263); for a 50-year-old male, 17533 evaluations took about 4 hours and 43 minutes and resulted in an optimal solution with RMS of R peak displacements 27.925 ms (SDNN of real RRI was 32.038). In both cases, the most optimal solutions did not have a penalty score. See **Table 1** for a list of the most optimal sets of personalized parameters.

The main result of our proposed concept is the time course of the R peak displacements (see parts C and F of **Figure 12** and **Figure 13** for 33 and 50-year-old males correspondingly). The R peak displacements of the 33-year-old male had a relatively stable baseline despite the real HR baseline drifts (see **Figure 12**A), even during shifts between resting and slow breathing periods. The R peak displacements had pulsations of about 0.1 Hz at multiple time intervals (see **Figure 12**F) that often resemble ABP (see **Figure 12**E) with a time delay of about 2.2 s. Furthermore, some R peak displacements overshot the mentioned pulsations just for a single RRI and these momentary heart decelerations were up to 280 ms compared to the expected by the personalized HR model (marked with red arrows in **Figure 12**F, e.g., the largest one appeared at 82 seconds). These decelerations often occurred at the rising part of slow R peak displacement pulsations after the previous drop of ABP with SNA burst (see **Figure 12**E) and expiration (see **Figure 12**D). In fact, in the 33 and 50-year-old male cases, SNA is generated more often and more strongly at drops in ABP via withdrawal of the modeled baroafferent activity (this is more clearly seen in **Figure 12**E). Meanwhile, baseline drifts existed in R peak displacements of 50-years-old male (**Figure 13**C). Here, R peak displacements did not resemble ABP in general, though few morphological similarities could also be envisioned, e.g., about 0.1 Hz pulsations at about 970–990 second and baseline drop at about 1060–1090 second intervals (compare **Figure 13** parts E and F). In both cases the time course of the R peak displacements was different from respiration, and especially in the 50-year-old male case the fast virtual HR variations mimicked respiration and the corresponding real HR patterns (see the parts D of **Figure 12** and **Figure 13**). Therefore, three main components of the R peak displacements may be visible to different individuals even during the same resting condition: very slow baseline drifts (<0.1 Hz), about 0.1 Hz pulsations, momentary fast irregularities.

4 Discussion

The concept of computerized physiology modeling followed in the article is based on the integration of basic physiology knowledge and cutting-edge computing technologies into virtual models. Virtual models allow not only to more effectively investigate physiological mechanisms, predict multiple influences, but also apply modeling results to biosignal and data processing, research, and clinical decision making (Pruett et al., 2020). This is especially relevant for the progress of personal medicine, prediction, and prevention. Modeling of HR regulation is an essential part of such approaches as virtual physiological human (www.vph-institute.org), or virtual patients for *in silico* trials (Sinisi et al., 2021). Article contributes for two main research problems in modeling of HR regulation: 1) how to integrate the abundant knowledge of physiology, psychology, and biophysics in

This is a provisional file, not the final typeset article

the form of formal models that are easily accessible to the user of computerized systems; and 2) how to enrich these models with additional empirical personal data, thereby refining the models and personalizing the decisions they could support.

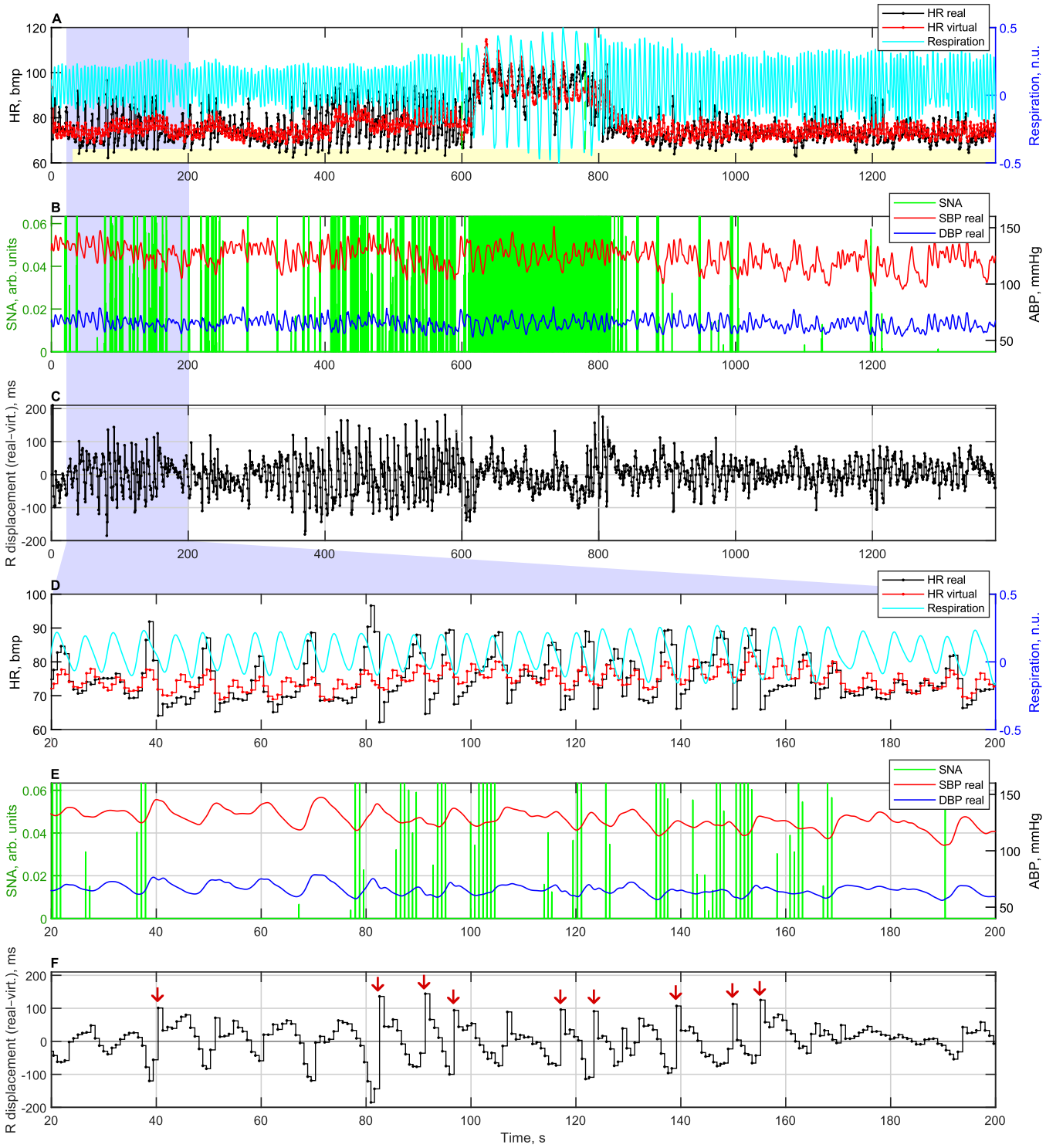

Figure 12. Psychophysiological data of a 33-year-old male: time course of the real and virtual heart rate (HR), respiration (A and D parts), the modeled sympathetic nerve activity (SNA), and the processed real arterial blood pressure (ABP) (B and E parts), R peak displacements (C and F parts). The A, B, and C parts are enlarged in D, E, and F. The period of slow respiration condition was from 600 to 780 second (green dashed marks in A part); other periods are in the resting state. HR model calibrated for period from 30 to 1380 second (light yellow strip at bottom of A part). Other abbreviations: DBP, diastolic blood pressure; SBP, systolic blood pressure.

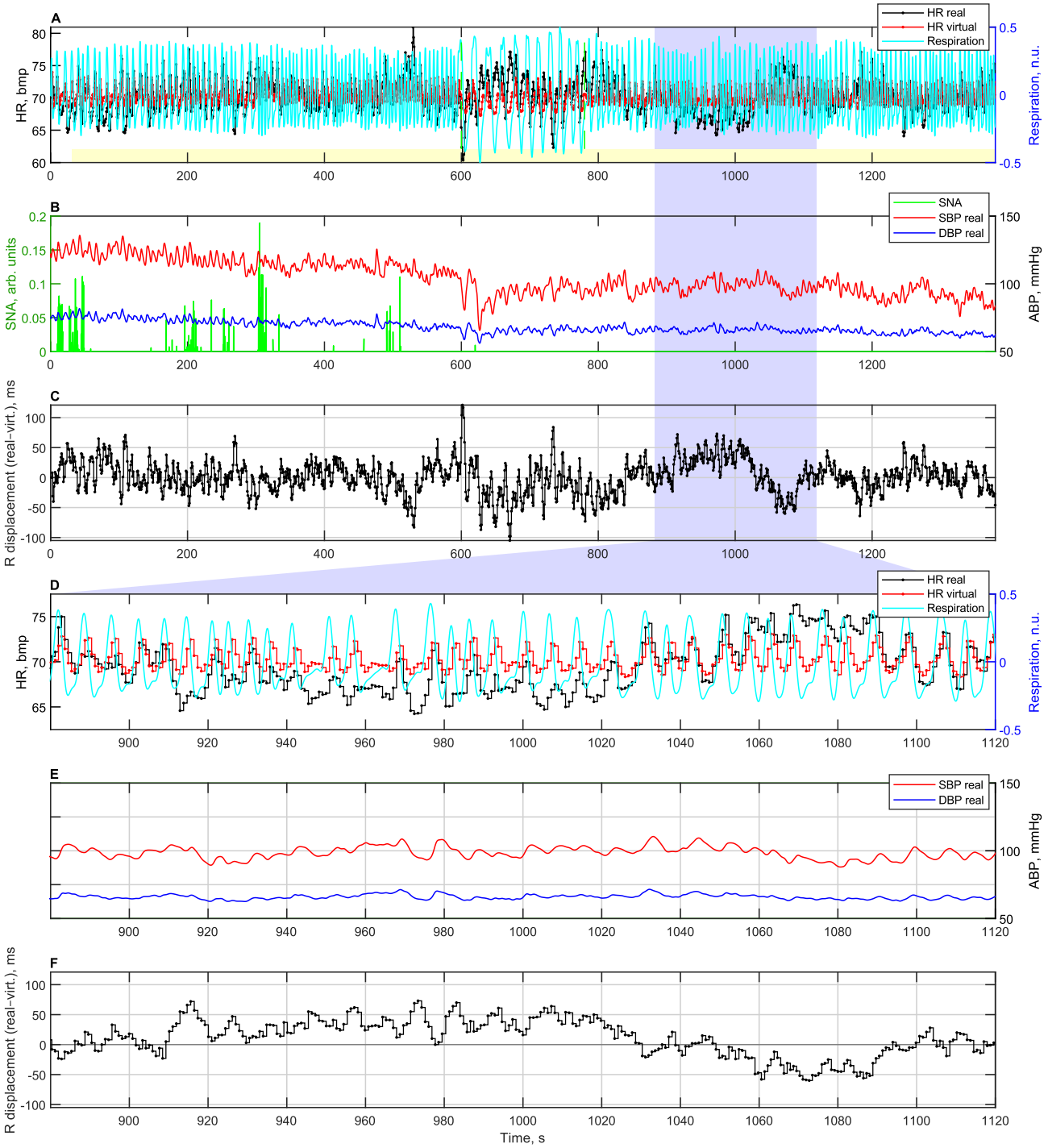

Figure 13. Psychophysiological data of a 50-year-old male: time course of the real and virtual heart rate (HR), respiration (A and D parts), the modeled sympathetic nerve activity (SNA), and the processed real arterial blood pressure (ABP) (B and E parts), R peak displacements (C and F parts). The A, B, and C parts are enlarged in D, E, and F. The period of slow respiration condition was from 600 to 780 second (green dashed marks in A part); other periods are in the resting state. HR model calibrated for period from 30 to 1380 second (light yellow strip at bottom of A part). Other abbreviations: DBP, diastolic blood pressure; SBP, systolic blood pressure.

The specific purpose of this paper was to present the concept of a computational method that could identify personalizable HR regulation parameters and capture the beat-by-beat variations (R peak displacements) that are expected to not be attributable to lower order HR regulation mechanisms –

This is a provisional file, not the final typeset article

respiratory arrhythmia and cardiac baroreflex. To our knowledge, such a method incorporating a multilevel model of HR regulation, designed to be fitted to empirical data and seeking to extract residual HR irregularities, has not yet been proposed. A valuable feature of the model is the presentation of neurophysiological regulatory mechanisms in the visual form of SIMULINK block diagrams, which makes the model and simulation easily interpretable.

In comparison – most of the available models allow modeling of generalized humans without availability to fit the model to the concrete person. There are also attempts to create patient-specific models (Gray and Pathmanathan, 2018), and the trend is to create more universal models suitable for either normal or pathological – personalized – conditions, paving the path from the virtual physiological human to the clinic (Hoekstra et al., 2018). One of popular models in MATLAB SIMULINK environment – PNEUMA (Hsing-Hua Fan and Khoo, 2002; Cheng et al., 2010), although highly elaborated, can simulate multiple influences even within heart period, however, it is too complex and would be too slow for search of parameters combinations for beat-to-beat personalization. Some newer models, relying on the knowledge of lower-level mechanisms, propose more elaborated neural regulations at relatively higher levels; for example, Park et al. (2020) model included more detailed parasympathetic activity regulation via NTS, NAmb, and dorsal motor nucleus of the vagus, but this is still about regulation at lower-order medulla oblongata level. Although HR regulation models involving multiple higher brain structures have already been described in the literature (Thayer and Lane, 2009; e.g. Smith et al., 2017), but they lack time axis and mathematical formulations.

To evaluate HR regulation influences, particularly those attributable to higher-order regulations, a model part of lower-order regulations should be adequate to the *in vivo* HRV. In particular, our proposed model was able to simulate RSA and cardiac baroreflex mimicking the morphology of the real HR. Our model personalization system was able to find parameter sets of HR model for two males encompassing two psychophysiological conditions – resting and slow breathing. Both different sets were useful to generate R peak displacements that are different from the respiration morphology, suggesting that the architecture of the RSA mechanism is adequate in our HR model.

Our proposed concept reveals the possibility to separate three components of R peak displacements and analyze them separately: tonic, spontaneous, and 0.1 Hz changes. The *tonic component*, like the baseline drifts seen in the 50-year-old male case, could be associated with slow changes in the mental, physiological, and humoral state. The *spontaneous changes* in the R peak displacements are seen in the 33-year-old male recording, while preliminary, suggests that there are possibly other factors here, perhaps sudden sporadically changed parasympathetic activity from higher-order areas of the brain, maybe partly due to additional interaction between baroinformation and RSA. The *0.1 Hz component* possibly related to Mayer waves, insufficient model adequacy in simulating the baroreflex from ABP. There is a 2.2 second delay of R displacements relative to the ABP (see **Figure 12** parts E and F) and it cannot be fitted to faster vagal or slower sympathetic baroreflex mechanisms – therefore the existing model could be improved by adding new mechanisms, their interactions, or additional input could be implemented. Nevertheless, interesting insights can come from analyzing components of R peak displacements extracted by our concept even as it is without modifications.

Our proposed model-based computational method has limitations and simplifications worth noting which may be improved in the future. One limitation is assuming the constant tonic level of ANS activity as higher-order neural control, although an effective input from the higher-order brain is expected at about 400–600 ms after EKG R as suggested from our previous study (Baranauskas et al., 2021). Also, our model currently does not simulate orthostatic hypotension; thus, this model is intended to be used when the person remains in the same posture. Furthermore, in our proposed approach, unexplained HR variations are provisionally attributed to higher-order brain regulation;

however, it could be attributed to any heart regulation level. Anyway, we believe that this approach could help investigate brain-heart interactions by enhancing the ratio between influences from brain and other HR regulation mechanisms. Future studies could try to discriminate sources of displacements of R peaks (e.g., higher-order neural or humoral; sympathetic or parasympathetic). Model-based computational system should be tested on a broader sample of subjects to reflect sex, age, and specific illnesses; for example, it is known that cardiac vagal baroreflex is relatively more pronounced in females and sympathetic baroreflex in males (Kim et al., 2011).

The model-based concept could be further applied to *in-silico* analysis of heart regulation in health care, medical diagnostics, psychology, and research of heart-brain interactions. The model parameters themselves could be useful for the assessment of respiratory arrhythmia and the baroreflex. R displacements could help control RSA and/or baroreflex effects in stress, fatigue, emotion studies or biofeedback systems while assessing tonic, phasic and/or spontaneous changes in HR. The model could help develop diagnostic and screening biomarkers (e.g., sympathovagal balance) based on HRV data retrieved from wearable devices. The developed computational system that integrates the psychophysiological mechanisms of HR regulation in the form of a formalized personalized model may facilitate further research and reveal new features of HR regulation that would be useful in practice.

Acknowledgments

The authors thank the Institute of Biomedical Electronics of the Vienna University of Technology for laboratory equipment for psychophysiological recordings. We thank Lena Kummer for her assistance in the experimental study. The authors thank all the volunteers for their participation in the study.

Conflict of Interest

The authors declare that the research was conducted in the absence of any commercial or financial relationships that could be construed as a potential conflict of interest.

Author Contributions

MB and RS contributed to conception. AL and MB contributed to funding acquisition. EK designed the pilot study for data collection. EK and MB did pilot study and collected the data. MB cared about modeling, software, data analysis, interpretation, visualization of results, and wrote the first draft of the manuscript. All authors contributed to manuscript revision, read, and approved the submitted version.

Funding information

This work was funded by the European Social Fund under No 09.3.3-LMT-K-712 “Development of Competences of Scientists, other Researchers and Students through Practical Research Activities” measure.

Ethics statement

Ethical approval was not provided for this study on human participants because pilot recordings are used as the basis for the ethic application (namely, for the estimation of the effect size and thus for the necessary size of the clinical study). The participants provided their written informed consent to

This is a provisional file, not the final typeset article

participate in this study. Written informed consent was obtained from the individuals for the publication of any potentially identifiable data included in this article.

Data Availability Statement

The raw data supporting the conclusions of this article will be made available by the authors, without undue reservation.

References

Albanese, A., Cheng, L., Ursino, M., and Chbat, N. W. (2016). An integrated mathematical model of the human cardiopulmonary system: model development. *Am. J. Physiol.-HEART Circ. Physiol.* 310, H899–H921. doi: 10.1152/ajpheart.00230.2014.

Bach, D. R., Castegnetti, G., Korn, C. W., Gerster, S., Melinscak, F., and Moser, T. (2018). Psychophysiological modeling: Current state and future directions. *Psychophysiology* 55, e13214. doi: 10.1111/psyp.13209.

Baranauskas, M., Grabauskaitė, A., Griškova-Bulanova, I., Lataitytė-Šimkevičienė, B., and Stanikūnas, R. (2021). Heartbeat evoked potentials (HEP) capture brain activity affecting subsequent heartbeat. *Biomed. Signal Process. Control* 68, 102731. doi: 10.1016/j.bspc.2021.102731.

Barman, S. M., and Yates, B. J. (2017). Deciphering the Neural Control of Sympathetic Nerve Activity: Status Report and Directions for Future Research. *Front. Neurosci.* 11. doi: 10.3389/fnins.2017.00730.

Berger, R. D., Saul, J. P., and Cohen, R. J. (1989). Transfer function analysis of autonomic regulation. I. Canine atrial rate response. *Am. J. Physiol. - Heart Circ. Physiol.* 256, H142–H152.

Borst, C., and Karemaker, J. M. (1983). Time delays in the human baroreceptor reflex. *J. Auton. Nerv. Syst.* 9, 399–409. doi: 10.1016/0165-1838(83)90004-8.

Cheng, L., Ivanova, O., Fan, H.-H., and Khoo, M. C. K. (2010). An integrative model of respiratory and cardiovascular control in sleep-disordered breathing. *Respir. Physiol. Neurobiol.* 174, 4–28. doi: 10.1016/j.resp.2010.06.001.

Chouchou, F., Mauguière, F., Vallayer, O., Catenoix, H., Isnard, J., Montavont, A., et al. (2019). How the insula speaks to the heart: Cardiac responses to insular stimulation in humans. *Hum. Brain Mapp.* 40, 2611–2622. doi: 10.1002/hbm.24548.

Coote, J. H. (2013). Myths and realities of the cardiac vagus. *J. Physiol.* 591, 4073–4085. doi: 10.1113/jphysiol.2013.257758.

Dergacheva, O., Griffioen, K. J., Neff, R. A., and Mendelowitz, D. (2010). Respiratory modulation of premotor cardiac vagal neurons in the brainstem. *Respir. Physiol. Neurobiol.* 174, 102–110. doi: 10.1016/j.resp.2010.05.005.

571 Draghici, A. E., and Taylor, J. A. (2016). The physiological basis and measurement of heart rate
572 variability in humans. *J. Physiol. Anthropol.* 35, 22. doi: 10.1186/s40101-016-0113-7.

573 Edwards, L., Ring, C., McIntyre, D., and Carroll, D. (2001). Modulation of the human nociceptive
574 flexion reflex across the cardiac cycle. *Psychophysiology* 38, 712–718. doi: 10.1111/1469-
575 8986.3840712.

576 Edwards, L., Ring, C., McIntyre, D., Winer, J. B., and Martin, U. (2009). Sensory detection
577 thresholds are modulated across the cardiac cycle: Evidence that cutaneous sensibility is
578 greatest for systolic stimulation. *Psychophysiology* 46, 252–256. doi: 10.1111/j.1469-
579 8986.2008.00769.x.

580 Feher, J. (2017). *Quantitative Human Physiology*. 2nd ed. Boston: Academic Press Available at:
581 https://www.sciencedirect.com/science/article/pii/B9780128008836000951.

582 Geus, E. J. C. de, Gianaros, P. J., Brindle, R. C., Jennings, J. R., and Berntson, G. G. (2019). Should
583 heart rate variability be "corrected" for heart rate? Biological, quantitative, and interpretive
584 considerations. *Psychophysiology* 56, e13287. doi: https://doi.org/10.1111/psyp.13287.

585 Gray, R. A., and Pathmanathan, P. (2018). Patient-Specific Cardiovascular Computational Modeling:
586 Diversity of Personalization and Challenges. *J Cardiovasc. Transl. Res.* 11, 80–88. doi:
587 10.1007/s12265-018-9792-2.

588 Guo, C. C., Sturm, V. E., Zhou, J., Gennatas, E. D., Trujillo, A. J., Hua, A. Y., et al. (2016).
589 Dominant hemisphere lateralization of cortical parasympathetic control as revealed by
590 frontotemporal dementia. *Proc. Natl. Acad. Sci.* 113, E2430–E2439. doi:
591 10.1073/pnas.1509184113.

592 Hoekstra, A. G., van Bavel, E., Siebes, M., Gijsen, F., and Geris, L. (2018). Virtual physiological
593 human 2016: translating the virtual physiological human to the clinic. *Interface Focus* 8. doi:
594 10.1098/rsfs.2017.0067.

595 Hsing-Hua Fan, and Khoo, M. C. K. (2002). PNEUMA - a comprehensive cardiorespiratory model.
596 in *Proceedings of the Second Joint 24th Annual Conference and the Annual Fall Meeting of*
597 *the Biomedical Engineering Society] [Engineering in Medicine and Biology*, 1533–1534
598 vol.2. doi: 10.1109/IEMBS.2002.1106522.

599 Ishbulatov, Y. M., Karavaev, A. S., Kiselev, A. R., Simonyan, M. A., Prokhorov, M. D.,
600 Ponomarenko, V. I., et al. (2020). Mathematical modeling of the cardiovascular autonomic
601 control in healthy subjects during a passive head-up tilt test. *Sci. Rep.* 10, 1–11. doi:
602 10.1038/s41598-020-71532-7.

603 Ishii, K., Mitsuhiro, I., and Matsukawa, K. (2015). Differential contribution of aortic and carotid
604 sinus baroreflexes to control of heart rate and renal sympathetic nerve activity. *J. Physiol. Sci.*
605 65, 471–480. doi: 10.1007/s12576-015-0387-2.

606 Jänig, W. (2006). *Integrative Action of the Autonomic Nervous System: Neurobiology of*
607 *Homeostasis*. Cambridge University Press.

This is a provisional file, not the final typeset article

Jose, A. D., and Collison, D. (1970). The normal range and determinants of the intrinsic heart rate in man. *Cardiovasc. Res.* 4, 160–167. doi: 10.1093/cvr/4.2.160.

Karemaker, J. M. (2022). The multibranched nerve: vagal function beyond heart rate variability. *Biol. Psychol.* 172, 108378. doi: 10.1016/j.biopsycho.2022.108378.

Kim, A., Deo, S. H., Vianna, L. C., Balanos, G. M., Hartwich, D., Fisher, J. P., et al. (2011). Sex differences in carotid baroreflex control of arterial blood pressure in humans: relative contribution of cardiac output and total vascular conductance. *Am. J. Physiol. - Heart Circ. Physiol.* 301, H2454–H2465. doi: 10.1152/ajpheart.00772.2011.

Koenig, J., Abler, B., Agartz, I., Åkerstedt, T., Andreassen, O. A., Anthony, M., et al. (2021). Cortical thickness and resting-state cardiac function across the lifespan: A cross-sectional pooled mega-analysis. *Psychophysiology* 58, e13688. doi: https://doi.org/10.1111/psyp.13688.

Kotani, K., Struzik, Z. R., Takamasu, K., Stanley, H. E., and Yamamoto, Y. (2005). Model for complex heart rate dynamics in health and diseases. *Phys. Rev. E* 72, 41904. doi: 10.1103/PhysRevE.72.041904.

Laborde, S., Mosley, E., and Thayer, J. F. (2017). Heart Rate Variability and Cardiac Vagal Tone in Psychophysiological Research – Recommendations for Experiment Planning, Data Analysis, and Data Reporting. *Front. Psychol.* 8. doi: 10.3389/fpsyg.2017.00213.

Magosso, E., Cavalcanti, S., and Ursino, M. (2002). Theoretical analysis of rest and exercise hemodynamics in patients with total cavopulmonary connection. *Am. J. Physiol.-Heart Circ. Physiol.* 282, H1018–H1034. doi: 10.1152/ajpheart.00231.2001.

Martins, A. Q., McIntyre, D., and Ring, C. (2014). Effects of baroreceptor stimulation on performance of the Sternberg short-term memory task: A cardiac cycle time study. *Biol. Psychol.* 103, 262–266. doi: 10.1016/j.biopsycho.2014.10.001.

Mather, M., Joo Yoo, H., Clewett, D. V., Lee, T.-H., Greening, S. G., Ponzio, A., et al. (2017). Higher locus coeruleus MRI contrast is associated with lower parasympathetic influence over heart rate variability. *NeuroImage* 150, 329–335. doi: 10.1016/j.neuroimage.2017.02.025.

Olufsen, M. S., and Ottesen, J. T. (2013). A practical approach to parameter estimation applied to model predicting heart rate regulation. *J. Math. Biol.* 67, 39–68. doi: 10.1007/s00285-012-0535-8.

Oppenheimer, S. M., Gelb, A., Girvin, J. P., and Hachinski, V. C. (1992). Cardiovascular effects of human insular cortex stimulation. *Neurology* 42, 1727–1732. doi: 10.1212/WNL.42.9.1727.

Ortiz-León, G., Vílchez-Monge, M., and Montero-Rodríguez, J. J. (2014). Simulations of the Cardiovascular System Using the Cardiovascular Simulation Toolbox. in *5th Workshop on Medical Cyber-Physical Systems* OpenAccess Series in Informatics (OASIcs)., eds. V. Turau, M. Kwiatkowska, R. Mangharam, and C. Weyer (Dagstuhl, Germany: Schloss Dagstuhl–Leibniz-Zentrum fuer Informatik), 28–37. doi: 10.4230/OASIcs.MCPS.2014.28.

Palma, J.-A., and Benarroch, E. E. (2014). Neural control of the heart: recent concepts and clinical correlations. *Neurology* 83, 261–271. doi: 10.1212/WNL.0000000000000605.

Pan, J., and Tompkins, W. J. (1985). A Real-Time QRS Detection Algorithm. *IEEE Trans. Biomed. Eng.* BME-32, 230–236. doi: 10.1109/TBME.1985.325532.

Park, J. H., Gorky, J., Ogunnaike, B., Vadigepalli, R., and Schwaber, J. S. (2020). Investigating the Effects of Brainstem Neuronal Adaptation on Cardiovascular Homeostasis. *Front. Neurosci.* 0. doi: 10.3389/fnins.2020.00470.

Pruett, W. A., Clemmer, J. S., and Hester, R. L. (2020). Physiological Modeling and Simulation—Validation, Credibility, and Application. *Annu. Rev. Biomed. Eng.* 22, 185–206. doi: 10.1146/annurev-bioeng-082219-051740.

Randall, E. B., Billeschou, A., Brinth, L. S., Mehlsen, J., and Olufsen, M. S. (2019). A model-based analysis of autonomic nervous function in response to the Valsalva maneuver. *J. Appl. Physiol.* 127, 1386–1402. doi: 10.1152/japplphysiol.00015.2019.

Sassi, R., Cerutti, S., Lombardi, F., Malik, M., Huikuri, H. V., Peng, C.-K., et al. (2015). Advances in heart rate variability signal analysis: joint position statement by the e-Cardiology ESC Working Group and the European Heart Rhythm Association co-endorsed by the Asia Pacific Heart Rhythm Society. *EP Eur.* 17, 1341–1353. doi: 10.1093/europace/euv015.

Schmaußer, M., Hoffmann, S., Raab, M., and Laborde, S. (2022). The effects of noninvasive brain stimulation on heart rate and heart rate variability: A systematic review and meta-analysis. *J. Neurosci. Res.* doi: 10.1002/jnr.25062.

Shaffer, F., and Ginsberg, J. P. (2017). An Overview of Heart Rate Variability Metrics and Norms. *Front. Public Health* 5. doi: 10.3389/fpubh.2017.00258.

Sinisi, S., Alimguzhin, V., Mancini, T., Tronci, E., and Leeners, B. (2021). Complete populations of virtual patients for in silico clinical trials. *Bioinformatics* 36, 5465–5472. doi: 10.1093/bioinformatics/btaa1026.

Smetana, P., and Malik, M. (2013). Sex differences in cardiac autonomic regulation and in repolarisation electrocardiography. *Pflüg. Arch. Eur. J. Physiol.* 465, 699–717. doi: 10.1007/s00424-013-1228-x.

Smith, R., Thayer, J. F., Khalsa, S. S., and Lane, R. D. (2017). The hierarchical basis of neurovisceral integration. *Neurosci. Biobehav. Rev.* 75, 274–296. doi: 10.1016/j.neubiorev.2017.02.003.

Spear, J. F., Kronhaus, K. D., Moore, E. N., and Kline, R. P. (1979). The effect of brief vagal stimulation on the isolated rabbit sinus node. *Circ. Res.* 44, 75–88. doi: 10.1161/01.RES.44.1.75.

Thayer, J. F., and Lane, R. D. (2009). Claude Bernard and the heart–brain connection: Further elaboration of a model of neurovisceral integration. *Neurosci. Biobehav. Rev.* 33, 81–88. doi: 10.1016/j.neubiorev.2008.08.004.

This is a provisional file, not the final typeset article

Ursino, M. (1998). Interaction between carotid baroregulation and the pulsating heart: a mathematical model. *Am. J. Physiol. - Heart Circ. Physiol.* 275, H1733–H1747.

Ursino, M., and Magosso, E. (2000). Acute cardiovascular response to isocapnic hypoxia. I. A mathematical model. *Am. J. Physiol.-Heart Circ. Physiol.* 279, H149–H165. doi: 10.1152/ajpheart.2000.279.1.H149.

Van Roon, A. M., Mulder, L. J. M., Althaus, M., and Mulder, G. (2004). Introducing a baroreflex model for studying cardiovascular effects of mental workload. *Psychophysiology* 41, 961–981. doi: 10.1111/j.1469-8986.2004.00251.x.

Wehrwein, E. A., and Joyner, M. J. (2013). "Chapter 8 - Regulation of blood pressure by the arterial baroreflex and autonomic nervous system," in *Handbook of Clinical Neurology* Autonomic Nervous System., ed. R. M. B. and D. F. Swaab (Elsevier), 89–102. Available at: http://www.sciencedirect.com/science/article/pii/B9780444534910000080 [Accessed April 22, 2016].

Wong, S. W., Massé, N., Kimmerly, D. S., Menon, R. S., and Shoemaker, J. K. (2007). Ventral medial prefrontal cortex and cardiovagal control in conscious humans. *NeuroImage* 35, 698–708. doi: 10.1016/j.neuroimage.2006.12.027.

Zeuzem, S., Olbrich, H. G., Seeger, C., Kober, G., Schöffling, K., and Caspary, W. F. (1991). Beat-to-beat variation of heart rate in diabetic patients with autonomic neuropathy and in completely cardiac denervated patients following orthotopic heart transplantation. *Int. J. Cardiol.* 33, 105–114. doi: 10.1016/0167-5273(91)90158-L.

Ziegler, G., Dahnke, R., Yeragani, V. K., and Bär, K.-J. (2009). The relation of ventromedial prefrontal cortex activity and heart rate fluctuations at rest. *Eur. J. Neurosci.* 30, 2205–2210. doi: 10.1111/j.1460-9568.2009.07008.x.